Superplastic behaviour of as received superplastic forming grade IN718 superalloy

B. P. Kashyap and M. C. Chaturvedi

Tensile specimens of superplastic forming grade IN718 superalloy, containing banded microstructure in the as received state, were deformed at high temperatures T to investigate the stress σ versus strain rate $\dot{\varepsilon}$ behaviour, the nature of the stress versus strain ε curves, ductility, and microstructure upon failure. The log σ–log $\dot{\varepsilon}$ plot for the $\dot{\varepsilon}$ range $\sim 5 \times 10^{-6}$–3×10^{-2} s^{-1} at $T = 1173$–1248 K exhibited a strain rate sensitivity index $m = 0{\cdot}62$ at low strain rates and $m = 0{\cdot}26$ at high strain rates, representing region II and III behaviour, respectively. The activation energies were estimated to be 308 and 353 kJ mol^{-1}, respectively. All the σ–ε curves, obtained at $\dot{\varepsilon} = 1 \times 10^{-4}$ s^{-1} for the temperature range 1173–1273 K, and at $T = 1198$ K for the strain rate range 1×10^{-4}–1×10^{-2} s^{-1}, exhibited initial flow hardening, followed by flow softening. The microstructures revealed dynamic recrystallisation, grain growth, cavitation, and a variation in the amount of second phase particles. Grain growth and cavitation were found to increase with temperature in region II. Excessive grain growth at 1273 K led to the elimination of region II. Grain growth and cavitation were both found to be less pronounced as the strain rate increased in region III.

MST/4377

At the time the work was carried out the authors were in the Department of Mechanical and Industrial Engineering, University of Manitoba, Winnipeg, Manitoba, Canada R3T 5V6, where Professor Kashyap was on leave from the Department of Metallurgical Engineering and Materials Science, Indian Institute of Technology, Bombay, Mumbai, 400 076, India. *Manuscript received 4 June 1999; accepted 5 August 1999.*

Introduction

Superplasticity is the ability of certain materials to exhibit exceptionally high ductility values of several hundred per cent under suitable microstructural and test conditions.[1] Initially the presence of fine equiaxed grains of size 10 μm or less was considered to be a prerequisite for this purpose. However, several materials, especially those processed by unidirectional mechanical working, contain non-equiaxed grains, which often remain stable when subjected to a reasonable static annealing. Such microstructures evolve into equiaxed fine grains of uniform distribution in the initial stages of deformation, under conditions otherwise appropriate for superplasticity.[2] Investigations of superplasticity in this group of materials provide an improved opportunity to evaluate the feasibility of superplastic formability in commercially produced materials. As superplastic forming is now a novel method for fabrication of various components, attempts are being made to convert other materials of interest into superplastic materials by modifying the composition and/or processing route. Superplastic forming (SPF) grade superalloy IN718 is one such material for aerospace applications. This material is used in turbine components, including those for the space shuttle, owing to a good combination of desired properties for parts such as compressors, turbine discs and rings, turbine shafts, exhaust sections, hot air ducting, and fasteners.

Superplasticity in IN718, having a maximum ductility of 294% and an associated strain rate sensitivity index m of 0·63, was reported by Chandler *et al.*[3] about 15 years ago. In a recent study by Smith and Flower,[4] the maximum ductility was observed to increase substantially depending on strain rate. This occurs in spite of cavitation and grain growth occurring during superplastic deformation.[5] In comparison with other superplastic materials, reported investigations on this material are very limited despite its commercial importance. To the present authors' knowledge, there does not appear to be any systematic study on superplasticity to delineate the effect of temperature on the nature of the stress–strain rate relationship and on ductility. Therefore, the aim of the present work on IN718 superalloy was first, to study the stress–strain rate behaviour and thereby establish the favourable conditions for superplasticity, and second, to optimise the conditions for maximum superplasticity. For this purpose, as received commercial SPF grade sheet, which contained a highly banded microstructure, was employed.

Experimental

The SPF grade IN718 superalloy was obtained in the form of 1·3 mm thickness sheet. The chemical composition (wt-%) was analysed to be Ni–17·4Cr–19·4Fe–4·99Nb–3·11Mo–1·07Ti–0·48Al–0·034C–0·19Cu.

For optical metallography, the samples were mechanically polished using Leco colloidal silica at the final stage. Cavities were examined in the as polished state. To observe the grain structure, the samples were electrolytically etched at room temperature in a solution of 10 g oxalic acid in 90 mL water. The etching time varied between 3 and 10 s at an applied potential of 6 V. Some of the samples were examined by SEM operating in the secondary electron mode.

Two sets of tensile specimens of gauge lengths 10 and 20 mm, but of the same gauge width of 5·4 mm, were machined. The first set of specimens was used to obtain the stress σ versus strain ε curves and ducility values at constant true strain rates $\dot{\varepsilon}$, and the second set of specimens was used to collect σ–$\dot{\varepsilon}$ data via the differential strain rate test technique. Tensile tests were conducted in air using a computer interfaced Instron universal testing machine. Heating and soaking for 30 min was carried out at the test temperature before deformation. Test temperature was controlled within an accuracy of ± 1 K.

Results

The microstructure of the as received sheet of SPF grade commercial IN718 superalloy is shown in Fig. 1. Figure 1*a* shows banding of very fine (sub)grains in three mutually

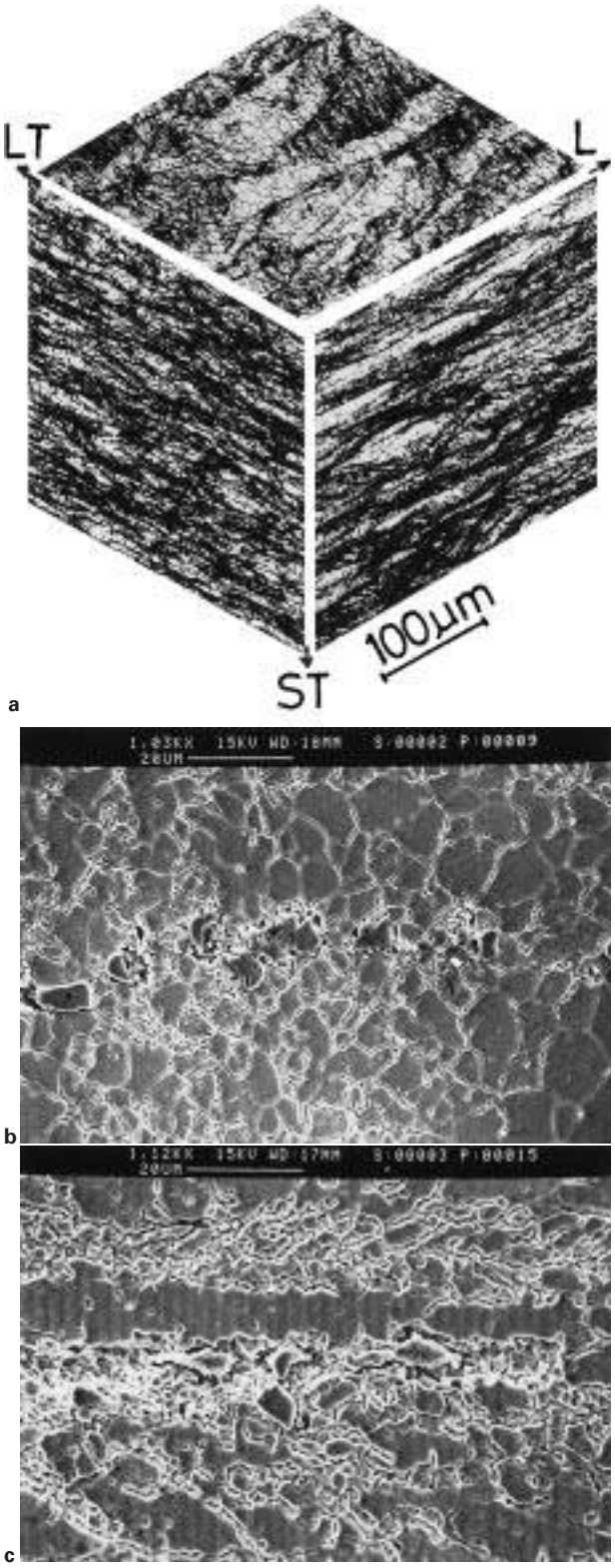

a optical, showing banding and heterogeneity (L longitudinal, LT long transverse, ST short transverse); *b* SEM, showing presence of precipitates in form of stringers (middle zone) in rolling plane; *c* as *b*, longitudinal plane

1 Microstructure of as received material

perpendicular surfaces. Whereas the bands on the rolling surface are observed to be relatively coarse, they are much finer on the longitudinal and transverse surfaces. When examined at higher magnification all the surfaces revealed a bimodal grain size distribution. On the rolling surface groups of coarse grains were surrounded by agglomerations of fine grains and vice versa, whereas in the longitudinal

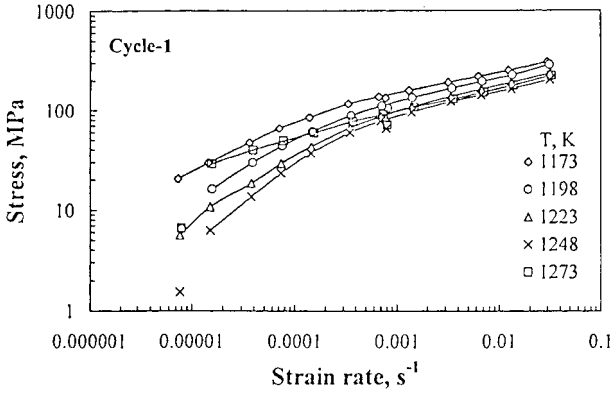

2 First cycle stress–strain rate data in log–log form at various temperatures *T*, exhibiting regions II and III

and transverse sections, layers of coarse grains were found to be arranged with a large number of fine grained layers between them. Typical distributions of grains on the rolling and longitudinal surfaces are presented in Fig. 1*b* and *c*. These micrographs also reveal typical agglomerations of second phase particles, some in the form of stringers, mainly in the direction of banding at the interfaces between the layers of coarse grains and fine grains. Using energy dispersive spectrometry (EDS) analysis these particles were found to be rich in niobium and they also contained carbon. Although it was not possible to quantify carbon, the EDS spectra suggested them to be NbC precipitates.

FLOW BEHAVIOUR

Tensile specimens, having the microstructures shown in Fig. 1, were deformed to study the flow behaviour at elevated temperatures as described below.

Stress–strain rate behaviour

Tensile specimens were deformed via the differential strain rate test technique over the strain rate range of about 5×10^{-6}–$3 \times 10^{-2}\,s^{-1}$ at constant temperatures in the range 1173–1273 K. The specimens were first deformed at an intermediate strain rate ($\sim 5 \times 10^{-4}\,s^{-1}$) before testing at all the strain rates in the selected range in sequence, from the lowest to the highest values. This approach was followed for two reasons, namely, (a) to avoid excessive time involvement in taking up the load at the lowest strain rate, due to the much lower load and the tendency for relaxation at high temperatures, and (b) to verify the occurrence of strain hardening or softening by repeating the starting strain rate. This whole sequence of strain rate changes, ending at the highest strain rate, will be referred to as cycle 1. Such differential strain rate testing was repeated on the same specimen to collect stress–strain rate data for cycles 2 and 3.

Figure 2 shows a plot of σ–$\dot{\varepsilon}$ data in log–log form for cycle 1 at various test temperatures T. As expected, the flow stress is observed to increase with strain rate. It can also be seen that the flow stress, at any selected strain rate, first decreases with increasing temperature in the range $T = 1173$–1248 K then tends to increase with further increases in temperature, especially for the lower strain rates. At any test temperature, a comparison of the two stress values at the same strain rate (repeated straining consisting of the starting rate and the seventh rate in ascending order from the lowest) reveal the occurrence of flow hardening during intermediate deformation. This can be seen to have become more prominent with increasing test temperature. Except at 1273 K, the σ–$\dot{\varepsilon}$ curves at all the test temperatures exhibit two regions, one with a greater slope in the lower strain rate range and another with a smaller slope in the higher strain rate range. The

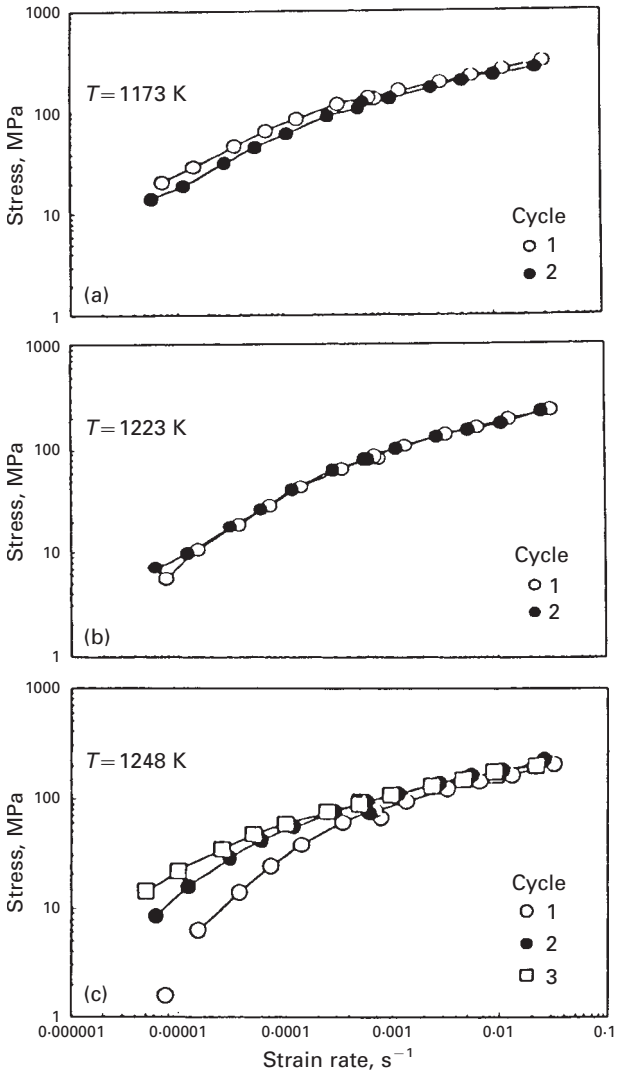

a $T = 1173$ K, showing flow softening; *b* $T = 1223$ K, showing neither flow hardening nor softening and thus suggesting pseudosteady state condition; *c* $T = 1248$ K, showing flow hardening

3 Effect of strain rate cycling on log(stress)–log(strain rate) plot at various temperatures *T*

values of these slopes m at different temperatures are given in Table 1. The values of $m = 0{\cdot}49$–$0{\cdot}80$ at lower strain rates and $m = 0{\cdot}23$–$0{\cdot}28$ at higher strain rates are typical of regions II and III for superplastic materials.

The plot of σ–$\dot{\varepsilon}$ data for cycle 2 was also found to exhibit the same general behaviour as discussed for cycle 1, namely, regions II and III were observed and the values of m are given in Table 1. However, the difference in flow stresses in the repeated strain rate test was reduced substantially. The plot of σ–$\dot{\varepsilon}$ data for cycles 1 and 2 together exhibited flow softening at 1173 K, steady state at 1198, 1223, and 1273 K, and flow hardening at 1248 K. Further cycling (cycle 3) led to steady state behaviour, if it was not already attained during cycle 2. The σ–$\dot{\varepsilon}$ plots representing the typical effects of strain rate cycling are shown in Fig. 3.

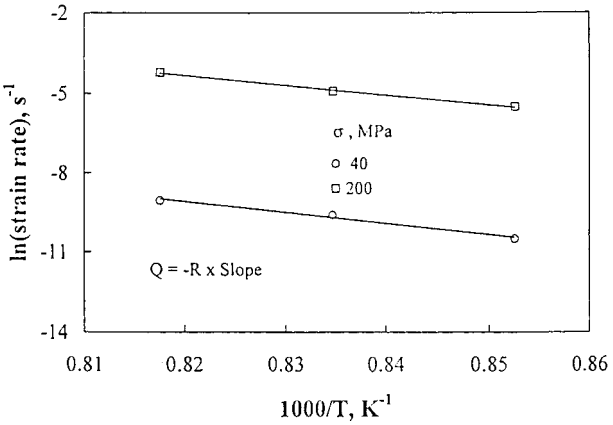

4 Arrhenius plot to determine activation energy for deformation in regions II and III within temperature range 1173–1223 K

In spite of the initial decrease followed by an increase in flow stress with increasing test temperature, an attempt to assess the existence of thermally activated deformation process was made using the data obtained at $T = 1173$–1223 K. Over this temperature range, there appears to be a distinct decrease in flow stress with increasing temperature. Arrhenius plots between $\ln \dot{\varepsilon}$ and $1/T$ at constant stresses of 40 and 200 MPa, corresponding to regions II and III, respectively, are presented in Fig. 4 from the cycle 1 σ–$\dot{\varepsilon}$ plot shown in Fig. 2. The slopes of straight lines in Fig. 4, when multiplied by the gas constant R, give the values of activation energy Q. The activation energies for deformation in regions II and III were thus estimated to be 308 and 353 kJ mol^{-1}, respectively.

Stress–strain curves

To study the effects of temperature and strain rate on the nature of the stress–strain curves and on ductility, tensile tests were conducted to failure at a constant strain rate of 1×10^{-4} s^{-1} and test temperatures of 1173–1273 K. At a constant temperature of 1198 K, tests were carried out at constant strain rates in the range 1×10^{-4}–1×10^{-2} s^{-1}. As shown in Fig. 5, flow hardening occurred during the early stages of deformation, followed by flow softening, irrespective of the test temperature and strain rate. It should be pointed out here that, under some test conditions, namely, $T = 1273$ K, $\dot{\varepsilon} = 1 \times 10^{-4}$ s^{-1}; $T = 1198$ K, $\dot{\varepsilon} = 5 \times 10^{-4}$ and 5×10^{-3} s^{-1}, the stress–strain curves exhibited a distinct yield drop. The flow stress can be seen to decrease with increasing temperature for $T = 1173$–1223 K. However, this trend is reversed for further increases in temperature. The values of the peak stresses σ_p and the strains corresponding to their occurrences ε_p under different test conditions are presented in Table 2. At intermediate temperatures, the σ–ε curves can be seen to approach steady state flow behaviour subsequent to flow softening. The σ–ε curves as a function of strain rate (Fig. 5*b*) exhibit an increase in stress with strain rate only in the early stage of deformation, and not towards the later stage.

Whereas the specimens deformed to study the effect of temperature failed in a pseudobrittle manner, those

Table 1 Values of strain rate sensitivity index in regions II m_{II} and III m_{III} at various test temperatures *T* and cycles

	T, K								
	1173		1198		1223		1248		1273
Cycle	m_{II}	m_{III}	m_{II}	m_{III}	m_{II}	m_{III}	m_{II}	m_{III}	m_{III}
1	0·49	0·23	0·60	0·28	0·68	0·28	0·80	0·27	0·26
2	0·52	0·24	0·54	0·26	0·60	0·28	0·69	0·24	0·25

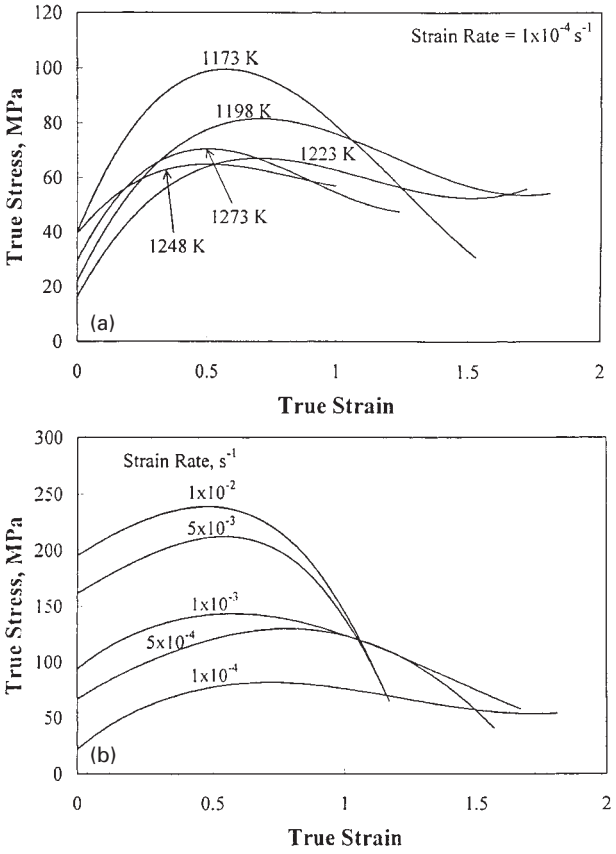

5 Stress–strain curves showing flow hardening followed by flow softening *a* at various temperatures ($\dot{\varepsilon} = 1 \times 10^{-4}\ s^{-1}$) and *b* at various strain rates ($T = 1198$ K): flow stress first decreases then increases with increasing temperature, whereas it increases monotonically with strain rate

deformed to investigate the effect of strain rate revealed sharp necking, especially at the higher strain rates. This is illustrated in Fig. 6 using the silhouettes of tensile specimens. As can be seen in Fig. 6*a* and Table 2, ductility $\Delta L/L_0$ (where ΔL is the change in gauge length and L_0 is the initial gauge length) first increases then decreases with increasing temperature, with a maximum ductility of 485% at $T = 1198$ K. As a function of strain rate (Fig. 6*b* and Table 2), ductility is observed to vary in an irregular manner, although the general tendency appears to suggest a decline in ductility with increasing strain rate, approaching a somewhat constant magnitude of about 221–225%.

MICROSTRUCTURES UPON DEFORMATION TO FAILURE

After deformation to failure the gauge sections of tensile specimens became very thin and hence only the

Table 2 Peak stress σ_p, corresponding strain ε_p, and ductility $\Delta L/L_0$ as function of temperature T at strain rate $\dot{\varepsilon} = 1 \times 10^{-4}\ s^{-1}$, and as function of strain rate at $T = 1198$ K

$\dot{\varepsilon}$, s^{-1}	T, K	σ_p, MPa	ε_p	$\Delta L/L_0$, %
1×10^{-4}	1173	104·0	0·595	348·2
	1198	85·3	0·746	485·3
	1223	69·8	0·808	468·0
	1248	70·7	0·470	380·2
	1273	66·0	0·455	179·0
1×10^{-4}	1198	85·3	0·746	485·3
5×10^{-4}		132·6	0·825	358·4
1×10^{-3}		145·8	0·641	466·3
5×10^{-3}		212·5	0·568	224·6
1×10^{-2}		239·7	0·488	220·6

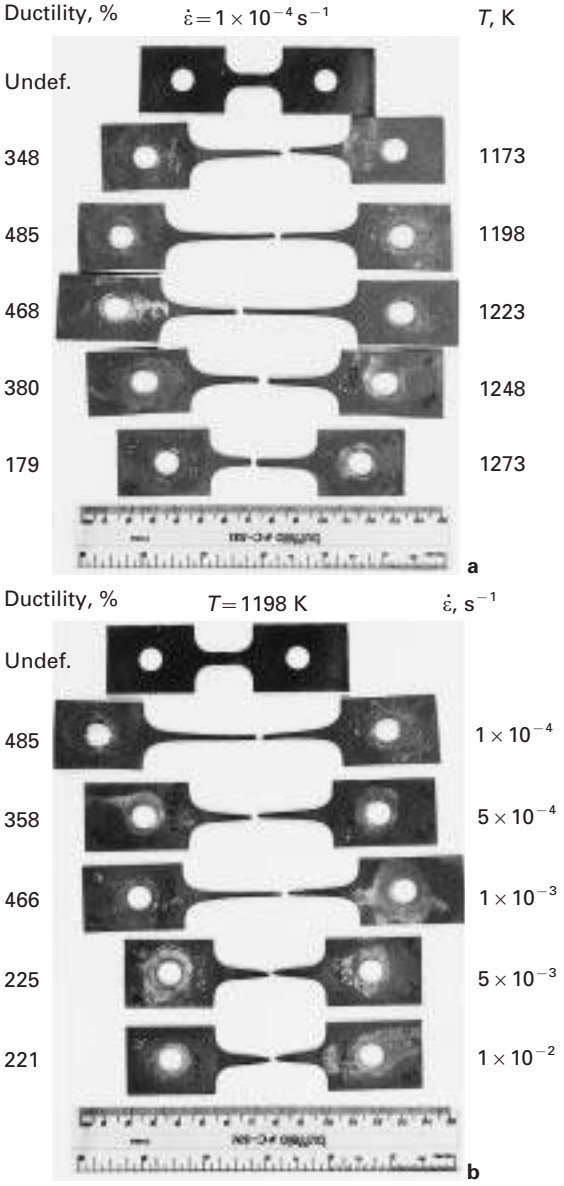

6 Silhouettes of specimens deformed to failure as function of *a* temperature ($\dot{\varepsilon} = 1 \times 10^{-4}\ s^{-1}$), showing pseudobrittle failure and *b* strain rate ($T = 1198$ K), showing necking at higher strain rates

longitudinal–long transverse (rolling) plane was examined for cavitation and grain structure. The specimens were found to cavitate to varying extents depending on the test conditions. Whereas the cavities were more or less uniformly distributed upon deformation at intermediate test temperatures (1198–1248 K) and lower strain rates (1×10^{-4}–$5 \times 10^{-4}\ s^{-1}$), under other test conditions they were mainly confined to near the fracture tips. As illustrated in Fig. 7, the amount of cavitation was found first to increase and then to decrease with increasing test temperature. Although the cavity size is noted to increase with temperature, the number of cavities appears first to increase and then to decrease as the temperature increases. With increasing strain rate, the level of cavitation was substantially reduced and no significant cavitation, except near the fracture tip, was noted towards the upper limit of the strain rate range investigated here. Figure 7*d* illustrates the cavities present upon deformation at the strain rate of $5 \times 10^{-3}\ s^{-1}$.

The specimens were examined at different magnifications after etching. At low magnifications, all the specimens, except that deformed at 1273 K, revealed a banded structure as illustrated in Fig. 8. At higher magnifications, the bands

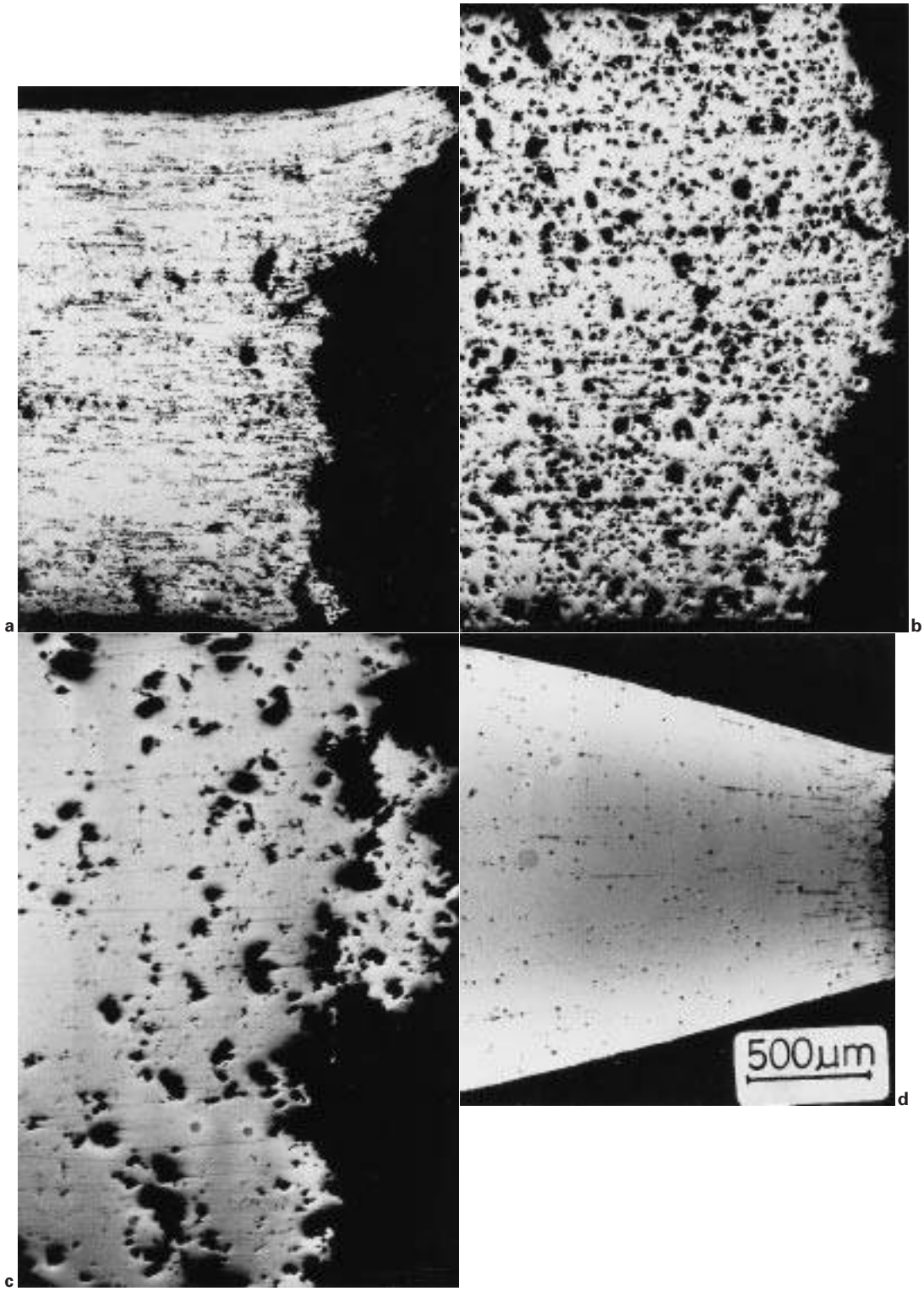

a $\dot{\varepsilon} = 1 \times 10^{-4}\ s^{-1}$, $T = 1198$ K; *b* $\dot{\varepsilon} = 1 \times 10^{-4}\ s^{-1}$, $T = 1248$ K; *c* $\dot{\varepsilon} = 1 \times 10^{-4}\ s^{-1}$, $T = 1273$ K; *d* $\dot{\varepsilon} = 5 \times 10^{-3}\ s^{-1}$, $T = 1198$ K

7 Variation in amount of cavitation on failure as function of test conditions: amount of cavitation increases with increasing temperature within superplastic region but is substantially reduced in region III (optical)

were found to contain cavities and irregular features which were prone to preferential etching. The interband region, which was observed to be almost featureless at low magnification, contained well defined grains and second phase particles distributed mainly along the grain boundaries and triple points. This is illustrated in Fig. 9*a*, which is a higher magnification image of the structure in Fig. 8. The effects of temperature and strain rate on microstructure are reported qualitatively, based on the observations at higher magnifications.

As exemplified in Fig. 9*a–c*, an increase in test temperature resulted in an increase in grain size with a simultaneous reduction in the number of second phase particles. Comparison of the micrographs in Fig. 9*a* and *c* shows a dramatic effect of temperature. The comparison of microstructures as a function of strain rate revealed a decrease in grain size with increasing strain rate. The grains, towards the upper limit of the strain rate range investigated, were very small as shown in Fig. 9*d*. The microstructures exhibited a more clearly delineated bimodal grain size

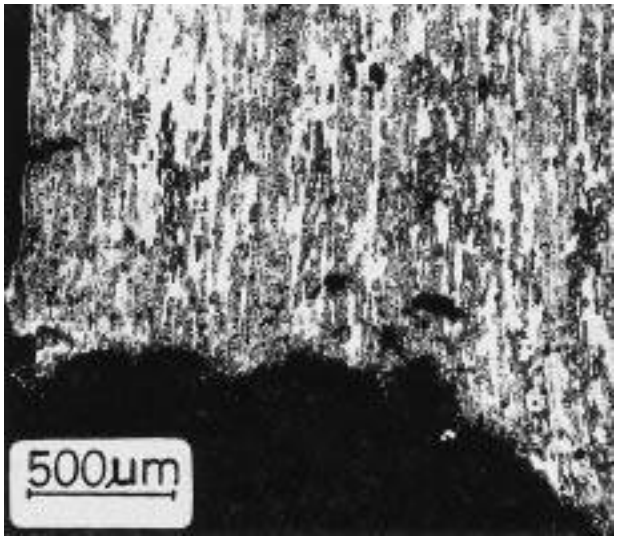

8 Image obtained after etching of same sample as shown in Fig. 7*a*, showing banded structure at low magnification (optical)

distribution with increasing strain rate. At the highest magnification employed for optical metallography in the present work, the second phase particles became less distinctly identifiable as the strain rate was increased.

Discussion

STRAIN SENSITIVE FLOW STRESS

Although a large number of studies on superplasticity involve the understanding of flow behaviour without attaching any significance to the effect of strain, there appears ample evidence of the variation in flow stress with strain, even in highly strain rate sensitive superplastic materials (e.g. *see* Refs. 2 and 6). The dependence of flow stress on strain can be seen to be dramatic in Fig. 5. The nature of the stress–strain curves is similar to that reported by Mahoney and Crooks[7] during superplastic deformation of IN718. Although no constant true strain rates were employed by Smith and Flower,[4] their study on SPF grade IN718 also revealed some variation in flow stress with strain. The effects of temperature and strain rate on the nature of the stress–strain curves found are similar to those reported[8] for IN744 microduplex stainless steel, which was also tested in a comparable microstructural state. During high temperature deformation of superplastic materials, the existence of such a non-steady state is generally attributed to concurrent microstructural evolution. Whereas grain growth during superplastic deformation leads to flow hardening, the evolution from initially elongated grains into equiaxed grains, dynamic recrystallisation, and cavitation are known to be responsible for flow softening.[6–10] Mahoney and Crooks[7] presented evidence for dislocation activity and dynamic recrystallisation during superplastic deformation of IN718 superalloy. Kashyap and Tangri[11] pointed out that the observed flow hardening in Al–Cu eutectic alloy could be accounted for only partly by concurrent grain growth whereas the balance could be due to conventional strain hardening. The latter can be even more important if, as in the present investigation, the microstructure does not contain well recrystallised grains initially (Fig. 1).

The nature of the stress–strain curves observed in the present investigation (Fig. 5) is comparable to that reported for materials undergoing continuous dynamic recrystallisation.[12] The first part of the stress–strain curves, where the flow stress increases with strain, is accordingly due to dynamic recovery. No TEM examination was made on the deformed specimens as a facility for more rapid cooling to arrest dislocations involved during deformation was not available. However, in the as received state, the grains/subgrains were reasonably free from dislocations. This implies that the generation and annihilation of dislocations occurred in the early stages of deformation. The initial part of the stress–strain curves (up to $\varepsilon \approx 0{\cdot}2$) in Fig. 5 can be seen to be linear, which suggests that only the generation of dislocations is important at this stage of deformation. Annihilation of dislocations becomes important when their density is increased beyond this strain. The decrease in strain hardening rate, measured via the deviation from initial linearity, represents thermally activated annihilation of dislocations. Under test conditions leading to a greater annihilation rate, the dislocation density will not increase sufficiently to attain the critical level required for recrystallisation and dynamic recrystallisation will be delayed. In IN718, Zhou and Baker[13] observed recrystallised grains at ε_p and so they concluded that recrystallisation had started before this strain was reached. The critical strain for dynamic recrystallisation is generally identified[12] as $\sim 0{\cdot}7\varepsilon_p$ but it is considered to be a reasonable approximation[14] to take ε_p as the critical strain. Zhou and Baker also reported that ε_p increased as strain rate increased and temperature decreased, which is in agreement with a previous report[15] on this subject. The variation in ε_p represented by the values given in Table 2, however, suggests it first increases then decreases as the strain rate and temperature are increased. Thus, dynamic recrystallisation is least favoured at intermediate strain rate and temperature. Similarly, the values of peak stress also do not show a systematic effect of temperature whereas Zhou and Baker found the Zener–Hollomon relation[16] to be valid. The two probable reasons for the differences in the results between the two investigations are as follows.

1. The initial microstructure in the present study was very fine and heterogeneous whereas the microstructures used by Zhou and Baker[13] were uniform, with a coarse grain size of 114 μm. The as received fine microstructure can undergo static recrystallisation and grain growth when the duration and temperature of treatment are adequate. Indeed, such an effect of static annealing was confirmed at the upper limit of the test temperatures employed in the present work. Then dynamic recovery and recrystallisation should be dictated by the grain size attained during the prior static grain growth and that during subsequent straining. Such an interactive effect will not have been present when deformation was started in the specimens which already contained coarse grain structure. In fact, the critical strain for onset of dynamic recrystallisation is engendered by a reduced grain size, owing to a more rapid rate of dislocation accumulation.[17]

2. The strain rate and temperature combinations employed by Zhou and Baker correspond to region III in the context of SPF grade material. Since the mechanisms for deformation in regions II and III are different, no monotonic effects of these variables can be expected on σ_p and ε_p over the entire ranges investigated.

To explain the increase in ε_p with increasing strain rate and decreasing temperature, which was observed for $\dot{\varepsilon} = 1 \times 10^{-4}$–$5 \times 10^{-4}\ s^{-1}$ and $T = 1223$–1273 K as given in Table 2, Zhou and Baker[13] applied the analysis utilised by Roberts.[17] According to this, the critical dislocation density required for the onset of dynamic recrystallisation increases with increasing strain rate and decreasing temperature. Therefore, the strain necessary to accumulate this critical dislocation density varies in the same manner. The opposite trend, for $\dot{\varepsilon} = 5 \times 10^{-4}$–$1 \times 10^{-2}\ s^{-1}$ and $T = 1173$–1223 K, evident in Table 2, may be due to the dominant effect of some other factors, such as the difference in the proportion of second phase particles noted after various deformation

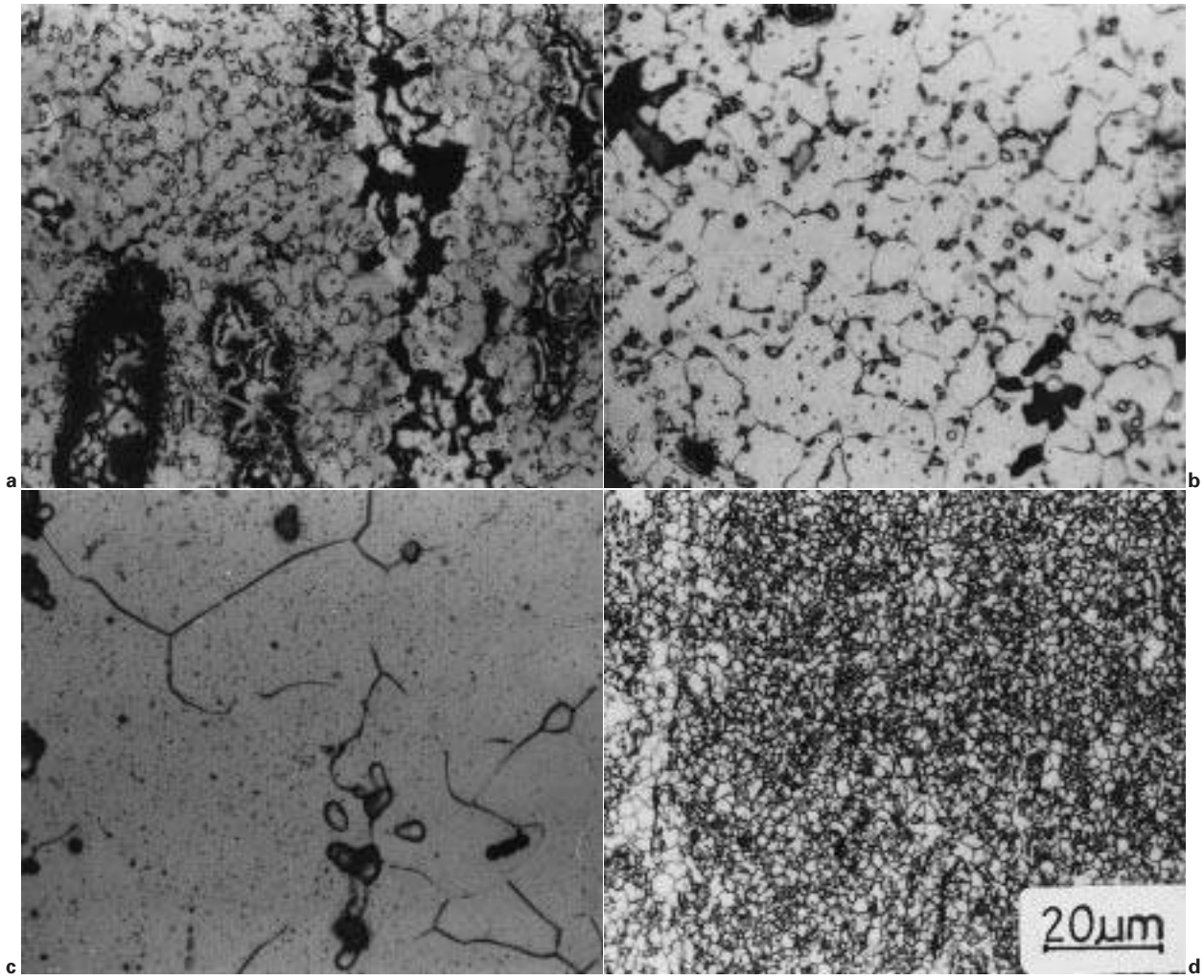

a $\dot{\varepsilon} = 1 \times 10^{-4}\ s^{-1}$, $T = 1198$ K; *b* $\dot{\varepsilon} = 1 \times 10^{-4}\ s^{-1}$, $T = 1248$ K; *c* $\dot{\varepsilon} = 1 \times 10^{-4}\ s^{-1}$, $T = 1273$ K; *d* $\dot{\varepsilon} = 5 \times 10^{-3}\ s^{-1}$, $T = 1198$ K

9 Variation in grain size and proportion of second phase particles on failure as function of test conditions: *a–c* reveal grain boundaries and second phase particles in interband region at high magnification in comparison with Fig. 8 and increasing grain size along with decreasing proportion of second phase particles as temperature increases, and *d* shows finer microstructure at higher strain rate (optical)

conditions. The proportion of these particles was observed to decrease with increasing temperature (Fig. 9) and was at a maximum at 1173 K. The presence of second phase particles would provide sites for generation and accumulation of dislocations, and therefore the critical dislocation density could be attained at a lower strain for a lower test temperature. Owing to the very fine microstructures of the specimens deformed at higher strain rates, this would not be a factor for such specimens.

ANOMALOUS EFFECT OF TEMPERATURE

During high temperature deformation, the flow stress is known to decrease with increasing temperature owing to the involvement of thermally activated processes such as grain boundary sliding, diffusion, dislocation climb, etc. The stress–strain curves in Fig. 5*a*, however, suggest that whereas this is observed in the temperature range 1173–1223 K, the flow stress becomes greater at the higher test temperatures (1248–1273 K). Also notable is the anomaly that the superplastic region disappears at 1273 K (Fig. 2), whereas on the basis of temperature alone superplastic behaviour would be expected to be present even at somewhat higher strain rates. The flow stress for superplastic deformation increases with grain size.[18] The micrographs in Fig. 9*a–c* reveal grain coarsening with increasing temperature. This can be ascribed to the enhanced grain boundary migration with increasing temperature as well as to the reduction in grain boundary pinning due to the smaller number of precipitates. The examination of precipitates using EDS suggested their composition to be Ni_3Nb (δ) and the matrix to be Υ phase. Zhou and Baker[13] identified such precipitates as δ phase in IN718 superalloy deformed at 1223 K. They also reported these precipitates to be absent upon deformation at higher temperatures. The absence of any systematic effect of temperature at higher temperatures may be due to the influence of both the grain size and precipitates. Whereas at 1248 K, the σ–$\dot{\varepsilon}$ plot (Fig. 2 and Table 1) exhibits superplasticity due to the small grain size, which is controlled by the optimum size and volume fraction of second phase particles, the whole range of the σ–$\dot{\varepsilon}$ plot at 1273 K reveals only region III behaviour. The deformation behaviour in region III is generally insensitive to grain size and this is the reason why the σ–$\dot{\varepsilon}$ plots for all the three cycles (not shown here) were comparable at 1273 K.

PARAMETERS OF CONSTITUTIVE RELATIONSHIP

In the present study, both the microstructural evolution and the variation in flow stress with strain are found to be substantial. Under such non-steady state conditions, the parameters of the constitutive relationship cannot be used to suggest the operating mechanisms for deformation, which are generally modelled on the basis of steady state

conditions.[19] However, the effect of non-steady state conditions appears to be much smaller on the stress–strain rate data obtained from differential strain rate tests (Fig. 2 and Table 1). The parameters of the constitutive relationship evaluated from these data can then provide a tentative explanation of the mechanisms for deformation. In region II, the average value of m (0·62 from Table 1) is comparable with that reported previously[3–5,7] during superplastic deformation of the present material. Furthermore, this is also comparable to the predictions of almost all the theories[19] of superplasticity ($m = 0{\cdot}5$). The experimental value of activation energy for superplastic deformation (353 kJ mol^{-1}) is closer to those typically obtained[12] for high temperature deformation of IN718 and Fe–Cr–Ni alloys (314–410 kJ mol^{-1}). However, this is much higher than the activation energy for grain boundary diffusion (107–198 kJ mol^{-1}: Ref. 20) in the major alloying elements present in this alloy. Therefore, it is suggested that whereas the conventional mechanism for superplastic deformation, namely, grain boundary sliding and its accommodation by grain boundary diffusion or dislocation climb at the grain boundaries, might be important in the regions containing fine equiaxed grains, the dislocation based mechanism should be operating within the grain interior of non-equiaxed and/or large grains. Indeed, Mahoney and Crooks[7] also presented evidence to suggest the superplastic flow in this alloy to be controlled by dislocation motion.

Since high temperature deformation behaviour at higher strain rates is known to be insensitive to grain size or, at most, only marginally dependent on grain size,[18,21] the stress–strain rate plots for different cycles were not markedly different (Fig. 3). In view of this observation, the values of the parameters of the constitutive relationship can be considered with some certainty to represent the mechanism for deformation. At higher strain rates, the average values of stress exponent ($n = 1/m = 3{\cdot}85$ or $m = 0{\cdot}26$) and the activation energy for deformation ($Q = 308$ kJ mol^{-1}) are both comparable to those reported previously[13] for creep and hot deformation. As pointed out in the 'Results' section above, such magnitudes of n and Q are representative of region III behaviour during high temperature deformation of superplastic materials. Based on these values of n and Q, the deformation is suggested to occur via dislocation creep.[22]

VARIATION IN DUCTILITY

With increasing temperature, ductility first increased then decreased (Fig. 6*a* and Table 2). Generally an increase in temperature has been known to improve ductility through its effect on thermally activated processes, associated with superplastic deformation. However, an increase in temperature can lead to grain growth, thereby limiting the ability of the material to exhibit superplasticity. In the present material, as the temperature increases the proportion of second phase particles can be seen to decrease along with concurrent grain growth and cavitation (Figs. 7–9). The increase in grain size is favourable for cavitation and therefore, as in the present work, both were found[21] to increase with temperature during superplastic deformation of Supral 220. However, it should be pointed out here that the cavities in IN718 were formed mostly by decohesion at particle/matrix interfaces and detailed study, presently in progress, may suggest some interrelationship amongst the various microstructural changes. From a preliminary study, Mahoney and Crooks[7] found the cavities to be associated with niobium carbide stringers. The maximum ductility observed at 1198 K may be the result of a favourable combination of microstructure and thermal activation for deformation. In two phase titanium alloys, the maximum in ductility has been reported to occur at some optimum proportion of α/β phases.[23] A similar effect is expected in an alloy system in which the existence of the second phase depends on precipitation/dissolution.

In spite of the decrease in grain size and reduction in cavitation level with increasing strain rate (Figs. 7 and 9), ductility is found to decrease (Fig. 6*b* and Table 2). The observed decrease in ductility with increasing strain rate is typical of the change from superplastic to conventional high temperature deformation behaviour. This is in general agreement with the decrease in the value of m from 0·62 in region II to 0·26 in region III. However, there exist some differences in the m values determined from the same set of experiments but using various methods of calculation.[24] This introduces some ambiguity in the precise relationship between ductility and m as a function of strain rate. Although no work was undertaken to examine the source of an irregular decrease in ductility with increasing strain rate at the lower end of the range used in the present study, it is notable that a similar variation in ductility is observed in the work of Smith and Flower.[4] The load–elongation curve obtained for this condition showed a distinct yield point, similar to that reported previously by Guimaraes and Jonas[15] in their detailed study.

Conclusions

1. Log σ–log $\dot{\varepsilon}$ plots over the strain rate range of $\sim 5 \times 10^{-6}$–3×10^{-2} s^{-1} exhibited region II and III type behaviour in the temperature range 1173–1248 K, and only region III at $T = 1273$ K. The values of m in regions II and III were found to be 0·62 and 0·26, respectively.

2. The stress–strain curves showed flow hardening followed by flow softening. Whereas the flow stress increased with strain rate, it first decreased then increased with increasing test temperature.

3. Dynamic recrystallisation, grain growth, and cavitation occurred during deformation. With increasing test temperature, the amount of second phase particles decreased whereas the grain size and the level of cavitation were both observed to increase under conditions of superplastic deformation. Upon deformation to failure at $T = 1198$ K, the grain size and cavitation level were both observed to decrease with increasing strain rate.

4. The maximum ductility of 485% was obtained at a strain rate of 1×10^{-4} s^{-1} and $T = 1198$ K. A decrease in ductility occurred with increasing temperature and strain rate. Whereas the former can be ascribed to concurrent grain growth and cavitation, the latter results from the change in the deformation mechanism, as indicated by a reduction in the magnitude of m from 0·62 to 0·26.

Acknowledgements

The authors would like to thank the consortium of Manitoba aerospace industries and the Natural Science and Engineering Research Council of Canada for financial support. One of the authors (BPK) would like to express thanks for the award of an Association of Commonwealth Universities Development Fellowship and to the Indian Institute of Technology, Bombay, for granting leave. Technical assistance by Mr D. Mardis and Mr J. Van Dorp is also gratefully acknowledged. The help provided by Dr W. Fan at different stages of the present work is highly appreciated.

References

1. J. W. EDINGTON, K. N. MELTON, and C. P. CUTLER: *Prog. Mater. Sci.*, 1976, **21**, 69–170.
2. M. SUERY and B. BAUDELET: *Rev. Phys. Appl.*, 1978, **13**, 53–66.

3. W. T. CHANDLER, A. K. GHOSH, and W. M. MAHONEY: *J. Spacecraft*, 1984, **21**, 61–64.
4. G. D. SMITH and H. L. FLOWER: *Adv. Mater. Process.*, 1994, **145**, (4), 32–34.
5. G. D. W. SMITH, S. R. GREGORY, Y. MA, Y. LI, and T. G. LANGDON: in 'Superalloys 718, 625, 706 and various derivatives', (ed. E. A. Loria), 303–314; 1997, Warrendale, PA, TMS.
6. A. K. GHOSH and C. H. HAMILTON: *Metall. Trans. A*, 1979, **10A**, 241–250.
7. M. W. MAHONEY and R. CROOKS: in 'Superplasticity in aerospace', (ed. H. C. Heikkenen and T. R. McNelley), 331–344; 1988, Warrendale, PA, TMS.
8. B. P. KASHYAP and A. K. MUKHERJEE: in 'Strength of metals and alloys', (ed. R. C. Gifkins), 707–712; 1982, Oxford, Pergamon Press.
9. B. P. KASHYAP, A. ARIELI, and A. K. MUKHERJEE: *J. Mater. Sci.*, 1985, **20**, 2661–2686.
10. B. P. KASHYAP and A. K. MUKHERJEE: *Res Mech.*, 1986, **17**, 293–355.
11. B. P. KASHYAP and K. TANGRI: *Metall. Trans. A*, 1987, **18A**, 417–424.
12. H. J. MCQUEEN and J. J. JONAS: in 'Plastic deformation of metals', (ed. R. J. Arsenault), 393–493; 1975, New York, Academic Press.
13. L. X. ZHOU and T. N. BAKER: *Mater. Sci. Eng. A*, 1994, **A177**, 1–9.
14. T. SAKAI and M. OHASHI: *Mater. Sci. Technol.*, 1990, **6**, 1251–1257.
15. A. A. GUIMARAES and J. J. JONAS: *Metall. Trans. A*, 1981, **12A**, 1655–1666.
16. C. ZENER and J. H. HOLLOMON: *J. Appl. Phys.*, 1944, **15**, 22–32.
17. W. ROBERTS: in 'Deformation, processing, and structure', (ed. G. Krauss), 109–184; 1984, Metals Park, OH, ASM.
18. T. G. LANGDON: *Metall. Trans. A*, 1982, **13A**, 689–701.
19. B. P. KASHYAP and A. K. MUKHERJEE: in 'Superplasticity', (ed. B. Baudelet and M. Suery), 4.1–4.34; 1985, Paris, CNRS.
20. E. A. BRANDES and G. B. BROOKS (eds.): in 'Smithells metals reference book', 7th edn, 13.1–13.119; 1992, Oxford, Butterworth-Heinemann.
21. J. PILLING and N. RIDLEY: in 'Superplasticity in crystalline solids', 65–70, 153–154; 1989, London, The Institute of Metals.
22. T. H. COURTNEY: in 'Mechanical behavior of materials', 263–324; 1990, New York, McGraw-Hill.
23. M. T. COPE, D. R. EVETTS, and N. RIDLEY: *J. Mater. Sci.*, 1986, **21**, 4003–4008.
24. K. A. PADMANABHAN and G. J. DAVIES: in 'Superplasticity', 30–38; 1980, Berlin, Springer-Verlag.